ACS APPLIED MATERIALS & INTERFACES

Research Article

www.acsami.org

Formation of Photoconductive Nanowires of Tetracene Derivative in Composite Thin Film

Tsuyoshi Suzuki,[†] Toshihiro Okamoto,*[,†,⊥] Akinori Saeki,[‡] Shu Seki,[‡] Hiroyasu Sato,[§] and Yutaka Matsuo*[,†]

[†]Department of Chemistry, School of Science, The University of Tokyo, 7-3-1 Hongo, Bunkyo-ku, Tokyo 113-0033, Japan

[‡]Department of Applied Chemistry, Graduate School of Engineering, Osaka University, 2-1 Yamadaoka, Suita, Osaka 565-0871, Japan

[§]Rigaku Corporation, 3-9-12 Matsubarachou, Akishima, Tokyo 196-8666, Japan

Supporting Information

ABSTRACT: Nanowires of tetracene dicarboxylic imide disulfide with an *N*-hexyl substituent (HexylTIDS) were successfully constructed in composite thin film containing poly(3-hexylthiophene) (P3HT). The nanowire structures were investigated by atomic force microscopy and scanning electron microscopy. The photoconductivity of the composite films was evaluated by time-resolved microwave conductivity measurements, revealing that the film containing a 1:1 w/w ratio of HexylTIDS and P3HT exhibited the highest photoconductivity (2.1×10^{-7} $m^2/(V\ s)$). The intermolecular interactions of HexylTIDS molecules were important in nanowire formation. These results suggest a one-step method for fabricating small-molecule-based nanowires in composite films from a blended solution. This type of composite film, and its fabrication method, will be useful for developing organic thin-film photoelectronic devices.

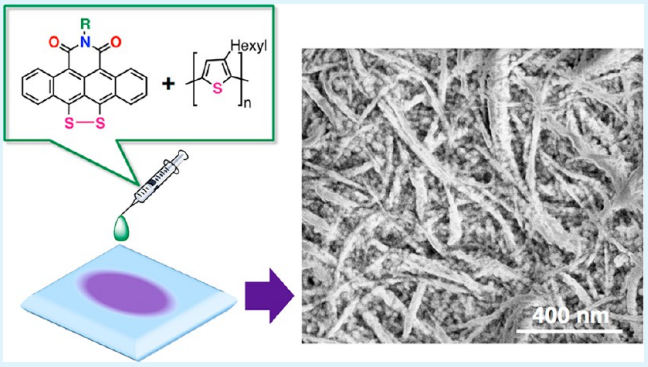

KEYWORDS: *organic semiconductor, tetracene, nanowire, intermolecular interaction, charge transport*

INTRODUCTION

Semiconducting organic π-conjugated materials have been widely studied toward realizing flexible, solution-processable, lightweight, and inexpensive electronic devices. Recently, one-dimensional micro- and nanosized aggregates of organic semiconductors have attracted much interest because of their versatile applications as optical waveguides,[1] fluorescent materials,[2] chemical sensors,[3] field-effect transistors,[4] and photodetectors.[5] In addition, the formation of nanowires in bulk heterojunction composite thin films has been studied for organic photovoltaics[6] and other organic electronics,[7] because nanowires provide large surface area and long conductive paths that enable efficient charge generation and transport. In these previous studies, π-conjugated polymers were normally used. A limited number of studies have been reported on small-molecule-based nanowires in composite films.[8] Furthermore, one-step formation of nanowires in composite films has been accomplished with only polymer components.[9] The difficulty of controlling the aggregation and packing structures of small molecules accounts for their limited use as nanowires in composite films, and spontaneous in situ formation of nanowires of small molecules in composite films is a challenging task.

In the present study, we investigated the formation of nanowires of tetracene imide disulfide (TIDS, Scheme 1) in

Scheme 1. Synthesis of TIDS

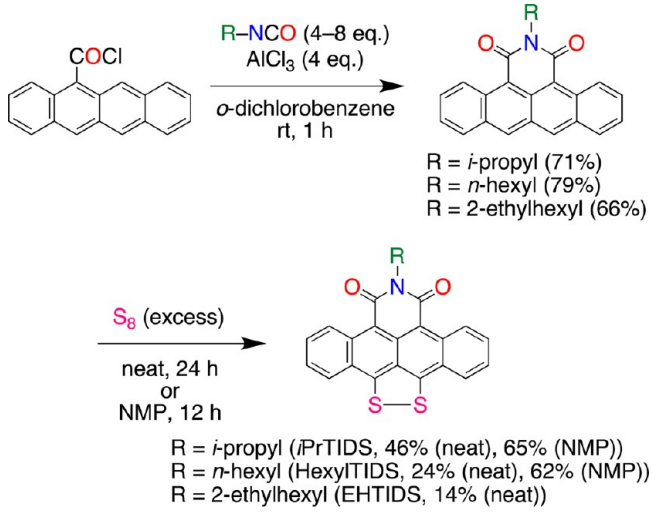

Received: September 11, 2012
Accepted: February 25, 2013
Published: February 25, 2013

composite films. The aggregation of TIDS molecules should be governed by $\pi-\pi$ interaction of the tetracene core, O···H interaction between the carbonyl group and aryl-H,[10] alkyl–alkyl interaction of *N*-substituents,[11] and chalcogen···chalcogen (S···O) interaction between the imide and disulfide groups,[12] as suggested from our previous report on TIDS with an isopropyl substituent (*i*PrTIDS).[13] In the present work, we found that a congener, hexyl-substituted TIDS (HexylTIDS), formed nanowires in composite films with poly(3-hexylthiophene) (P3HT). Herein we report the in situ one-step fabrication of nanowires of HexylTIDS in composite films and their photoconductivity. This aggregation structure should be useful for improving the performance of organic electronics.[14]

EXPERIMENTAL SECTION

General. All the reactions were carried out under an atmosphere of nitrogen. Air- or moisture-sensitive liquids and solutions were transferred via a syringe or a cannula. Melting points of solid materials were determined on a Mel-Temp capillary melting-point apparatus and were uncorrected. Analytical thin-layer chromatography (TLC) was performed on a glass plates with 0.25 mm 230–400 mesh silica gel containing a fluorescent indicator (MERCK Silica gel 60 F254). TLC plates were visualized by exposure to ultraviolet lamp (254 and 365 nm). Flash column chromatography was performed on Wakogel C200 (75–150 μm). All NMR spectra were taken at 500 MHz (JEOL ECA-500 spectrometer). Routine mass spectra were acquired by atmospheric pressure ionization (APCI) using a quadrupole mass analyzer on JEOL JMS-T100LC (AccuTOF) spectrometer and fast atom bombardment (FAB) on a JEOL JMS 700P FAB-MS spectrometer. NMR spectra were recorded in parts per million (ppm, δ scale) from residual protons of the deuterated solvent for ^{1}H NMR (δ 7.26 ppm for chloroform) and from solvent carbon for ^{13}C NMR (δ 77.16 ppm for chloroform). The data were presented as following space: chemical shift, multiplicity (s = singlet, d = doublet, t = triplet, m = multiplet, and/or multiplet resonances), coupling constant in hertz (Hz), and signal area integration in natural numbers, assignment (italic). Elemental analysis was performed at the University of Tokyo, Department of Chemistry, Organic Elemental Analysis Laboratory. UV–vis absorption was measured with JASCO V-670. AFM graphics were taken by a Seiko Instrument Inc., SPA 400, Soundproof Housing.

Materials. Tetracene, *n*-butyllithium (*ca.* 1.6 mol/L in hexane), and isocyanate derivatives were purchased from TCI. *N*-bromosuccinimide (NBS) and aluminum trichloride were purchased from Sigma–Aldrich Inc. NBS was recrystallized from water prior to use. Thionyl chloride, sulfur, and solvents were purchased from KANTO chemicals. *o*-Dichlorobenzene was purified by a solvent purification system (GlassContour)[15] equipped with columns of activated alumina and supported copper catalyst (Q-5) prior to use. 5-Tetracenecarbonyl chloride, *N*-isopropyl tetracene 5,6-dicarboxylic acid imide and *N*-isopropyl tetracene 5,6-dicarboxylic acid imide 11,12-disulfide (*i*PrTIDS) were synthesized in the same methods to our previous work.[13]

Synthesis of *N*-(Alkyl)-tetracenecarboxylic Acid 5,6-Imide. To a suspension of $AlCl_3$ (4.0 equiv) in *o*-dichlorobenzene (1.0 M) was added *o*-dichlorobenzene solution (0.25 M) of 5-tetracenecarboxyl chloride dropwise at room temperature. The color of the reaction mixture turned to dark green immediately. The mixture was poured into a solution of hexyl isocyanate (4.0 equiv) in *o*-dichlorobenzene (1.0 M). After stirring for 2 h at room temperature, the reaction mixture was poured into water, extracted with $CHCl_3$ by three times, washed with water, filtered, and concentrated under reduced pressure. After the crude product was dissolved in small amount of $CHCl_3$, MeOH was added to reprecipitate deep purple solids, which were dried under reduced pressure with P_2O_5 to give pure target compound.

Data for *N*-(*n*-hexyl)-tetracenecarboxylic acid 5,6-imide: 2.22 g (5.82 mmol, 79% yield). R_f = 0.60 (silica gel, $CHCl_3$). Mp 189.2–190.2 °C. ^{1}H NMR (500 MHz, $CDCl_3$): δ 10.14 (d, J = 9.0 Hz, 2H, Ar*H*), 9.11 (s, 2H, Ar*H*), 8.15 (d, J = 9.0 Hz, 2H, Ar*H*), 7.85 (dd, J = 6.0 Hz, 6.0 Hz, 2H, Ar*H*), 7.60 (t, J = 6.0 Hz, 2H, Ar*H*), 4.41 (t, J = 8.0 Hz, 2H, NCH_2CH$_2$), 1.88 (m, 2H, NCH$_2$CH_2), 1.39 (m, 4H, CH_2CH_2CH$_3$), 0.91 (t, J = 7.0 Hz, CH$_2$CH_3). ^{13}C{^{1}H} NMR (125 MHz, $CDCl_3$): δ 164.28, 144.96, 137.11, 134.82, 131.72, 131.03, 129.32, 126.85, 125.95, 125.77, 114.08, 41.00, 31.72, 28.27, 27.14, 22.71, 14.11. HRMS (APCI+) Calcd for $C_{26}H_{24}NO_2$ (MH^+) 382.1807. Found 382.1798. IR (ZnSe): 1664, 1627.

Data for *N*-(2-ethylhexyl)-tetracenecarboxylic acid 5,6-imide: 1.24 g (3.03 mmol, 66% yield). R_f = 0.45 (silica gel, $CHCl_3$/hexane = 4:1). Mp 120.0–120.7 °C. ^{1}H NMR (500 MHz, $CDCl_3$): δ 10.09 (d, J = 9.2 Hz, 2H, Ar*H*), 9.09 (s, 2H, Ar*H*), 8.14 (d, J = 9.7 Hz, 2H, Ar*H*), 7.84 (dd, J = 8.0 Hz, 8.0 Hz, 2H, Ar*H*), 7.60 (t, J = 8.0 Hz, 2H, Ar*H*), 4.38 (m, 2H, NCH_2CH), 2.12 (m, 1H, NCH$_2$C*H*), 1.55–1.29 (m, 8H, NCH$_2$CH(CH_2CH$_3$)CH_2CH_2CH_2CH$_3$), 0.98 (t, J = 8.0 Hz, CH$_2$CH_3), 0.88 (t, J = 8.0 Hz, CH$_2$CH_3). ^{13}C{^{1}H} NMR (125 MHz, $CDCl_3$): δ 164.89, 137.21, 135.05, 131.80, 131.32, 129.45, 127.49, 127.04, 126.28, 125.85, 114.55, 44.43, 37.95, 30.84, 28.70, 24.12, 23.21, 14.11, 10.79. HRMS (FAB+) calcd for $C_{28}H_{27}NO_2$ (M^+): 409.2042. Found: 409.2065. IR (ZnSe): 1668, 1629.

Synthesis of *N*-(Alkyl)-tetracenecarboxylic Acid 5,6-Imide-11,12-disulfide (TIDS). *Method a.* A mixture of *N*-(alkyl)-tetracenecarboxylic acid 5,6-imide and sulfur (100 mol amt. excess) was heated at 210–220 °C under nitrogen for 24 h. The reaction mixture was allowed to cool to room temperature. The crude product was subjected to silica gel column chromatography (eluent: CS_2, toluene, then $CHCl_3$/acetone = 49/1) to give TIDS as blue solids.

Method b. *N*-(alkyl)-tetracenecarboxylic acid 5,6-imide and sulfur (100 mol amt. excess) was dissolved in NMP (50 mM) and heated at 180 °C under nitrogen for 12 h. The dark green reaction mixture was poured into MeOH to precipitate blue solids. It was filtered and washed with CS_2 to remove excess amount of sulfur to give TIDS as blue solids.

Data for *N*-(*n*-hexyl)-tetracenecarboxylic acid 5,6-imide-11,12-disulfide (HexylTIDS): (*method a*) 109 mg (0.246 mmol, 24% yield). (*method b*) 718 mg (1.62 mmol, 62% yield). R_f = 0.50 (silica gel, $CHCl_3$/acetone =49/1). Mp 287.3–288.5 °C. ^{1}H NMR (500 MHz, $CDCl_3$): δ 10.22 (d, J = 9.0 Hz, 2H, Ar*H*), 7.89 (d, J = 8.0 Hz, 2H, Ar*H*), 7.83 (t, J = 7.5 Hz, 2H, Ar*H*), 7.52 (t, J = 7.5 Hz, 2H, Ar*H*), 4.37 (t, J = 7.5 Hz, 2H, NCH_2CH$_2$), 1.84 (m, 2H, NCH$_2$CH_2), 1.39 (m, 4H, CH_2CH_2CH$_3$), 0.91 (t, J = 7.0 Hz, 3H, CH$_2$CH_2CH_3). ^{13}C{^{1}H} NMR (125 MHz, $CDCl_3$): δ 163.50, 158.24, 135.67, 132.97, 129.44, 128.12, 126.51, 125.34, 125.26, 123.67, 107.97, 41.08, 31.78, 28.11, 27.24, 22.75, 14.13. MS (APCI+) 444.1424. IR (ZnSe): 1644, 1599. Anal. calcd for $C_{26}H_{21}NO_2S_2$: C, 70.40; H, 4.95; N, 3.16. Found: C, 70.30; H, 4.77; N, 2.99.

Data for *N*-(2-ethylhexyl)-tetracenecarboxylic acid 5,6-imide-11,12-disulfide (EHTIDS): (*method a*) 188 mg (0.399 mmol, 14% yield) after GPC purification (eluent: $CHCl_3$). R_f = 0.66 (silica gel, $CHCl_3$/acetone =49/1). Mp 217–218 °C. ^{1}H NMR (500 MHz, $CDCl_3$): δ 10.22 (d, J = 9.0 Hz, 2H, Ar*H*), 7.92 (d, J = 8.0 Hz, 2H, Ar*H*), 7.84 (t, J = 7.3 Hz, 2H, Ar*H*), 7.53 (t, J = 7.3 Hz, 2H, Ar*H*), 4.41–4.32 (m, 2H, NCH_2CH), 2.13–2.08 (m, 1H, NCH$_2$C*H*), 1.55–1.25 (m, 6H, NCH$_2$CH(CH_2CH$_3$)CH_2CH_2CH$_3$), 0.96 (t, J = 7.0 Hz, 3H, CH$_2$CH_3), 0.87 (t, J = 7.0 Hz, 3H, CH$_2$CH_3). ^{13}C{^{1}H} NMR (125 MHz, $CDCl_3$): δ 163.35, 157.24, 134.82, 132.40, 128.50, 127.75, 127.61, 124.66, 124.59, 122.69, 107.20, 44.47, 37.95, 30.91, 28.71, 24.20, 23.35, 14.21, 10.89. IR (ZnSe): 1655, 1617. Anal. calcd for $C_{28}H_{25}NO_2S_2$: C, 71.31; H, 5.34; N, 2.97. Found: C, 71.16; H, 5.43; N, 2.83.

X-ray Crystal Structural Analysis. Blue needle single-crystals of HexylTIDS were made by physical vapor transportation method with argon gas flowing.[16] Single crystal X-ray structural measurement was performed on Rigaku R-AXIS RAPID II and Rigaku AFC-8 diffractometers. Crystal data for HexylTIDS: $C_{26}H_{21}NO_2S_2$, M_r = 443.58, a blue needle, 0.65 mm × 0.09 mm × 0.03 mm, monoclinic, $P21/c$, a = 5.05464(9), b = 23.4235(4), c = 16.7903(3) Å, β = 90.676(6)°, V = 1987.79(6) Å^3, Z = 4, D_{calcd} = 1.482 g cm^{-3}, μ = 2.630 cm^{-1} (Cu Kα), $F(000)$ = 928.00, λ = 1.54187 Å, T = 93 K, R_1 = 0.0397

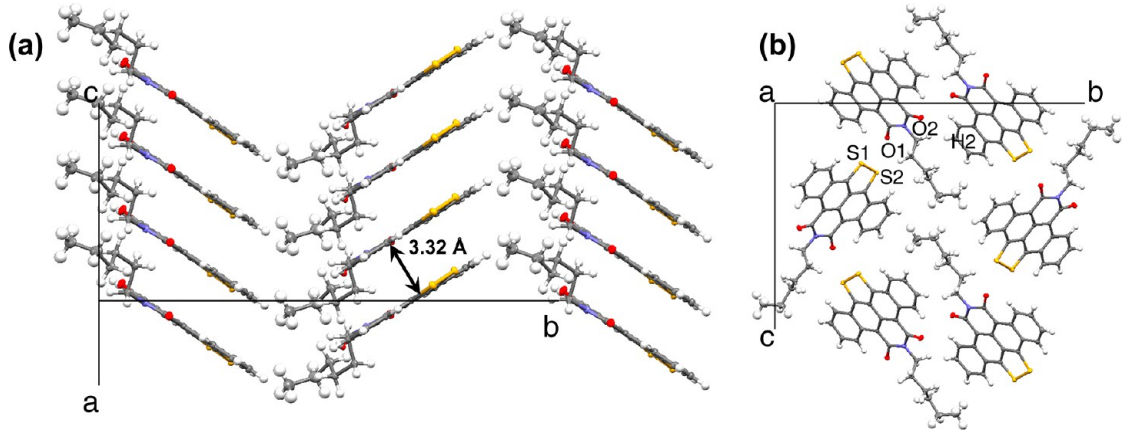

Figure 1. Packing structures of HexylTIDS: (a) side view, (b) top view.

$[I > 2\sigma(I)]$, wR_2 = 0.1119 [all reflections], GOF = 1.120, 3573 independent reflections and 281 parameters.

Preparation for TIDS:P3HT Composite Films and TIDS Films. Prior to use, quartz plates were cleaned by ultrasonication with a surfactant and rinsed with water. Poly(3-hexylthiophene) (P3HT) was purchased from Aldrich and used without further purification. P3HT and TIDS derivatives were dissolved in chlorobenzene at 80 °C separately. The concentrations were 0.3 wt % for P3HT, HexylTIDS and EHTIDS solutions and 0.1 wt % for an *i*PrTIDS solution. The solutions were mixed into several weight ratios at 80 °C. The hot mixture solutions were drop-casted onto the quartz plates and dried under reduced pressure. TIDS films were fabricated from corresponding TIDS solutions without mixing with P3HT through the same manner.

Scanning Electron Microscopy (SEM). Organic films on quartz plates were used without metal nanoparticle sputter coating. The films were fixed onto a metal stage with aluminum attachment. SEM measurements were carried out on Magellan 400L provided by FEI Company. The samples were measured under less than 1×10^{-4} Pa with around 1 mm in working distance. The acceleration voltage was 1.00 kV, and current was 13 pA for an electron beam.

Flash-Photolysis Time-Resolved Microwave Conductivity (FP-TRMC) Method. FP-TRMC measurements were carried out at 25 °C in air, where the resonant frequency and microwave power were properly adjusted at 9.1 GHz and 3 mW, respectively. Charge carriers were photochemically generated using a third harmonic generation (THG, 355 nm) light pulse from a Spectra-Physics model INDI Nd:YAG laser with a pulse duration of 5−8 ns. The excitation photon density was $4.6 \times 10^{15}/(\mathrm{cm}^2\ \mathrm{pulse})$. Transient conductivities ($\Delta\sigma$) were evaluated according to $\Delta\sigma = (1/A)(\Delta P_r/P_r)$, where A, ΔP_r, and P_r represent sensitivity factor, change of reflected microwave power, and reflected microwave power, respectively. Subsequently, $\Delta\sigma$ was converted to the product of the quantum yield: ϕ and the sum of charge carrier mobilities: $\sum\mu$ ($= \mu_h + \mu_e$) by $\phi\sum\mu = \Delta\sigma(eI_0F_{light})^{-1}$, where e, I_0, and F_{Light} are the unit charge of a single electron, incident photon density of excitation laser (photons m^{-2}), and a correction (or filling) factor (m^{-1}), respectively.[17]

RESULTS AND DISCUSSION

1. Synthesis and Packing Structure. TIDS with *N*-hexyl and *N*-2-ethylhexyl chains (HexylTIDS and EHTIDS, Scheme 1) were prepared according to our previous paper describing the synthesis of *i*PrTIDS.[13] Friedel−Crafts-type reactions using 5-tetracene carboxyl chloride, *N*-alkyl isocyanate, and $AlCl_3$ were conducted to obtain intermediate *N*-(alkyl)-tetracene dicarboxylic acid 5,6-imides. TIDS were obtained by the neat reaction of these intermediates with elemental sulfur at over 200 °C or in *N*-methylpyrrolidone (NMP) at 180 °C. The use of this solvent gave higher yield in a shorter reaction time. UV−vis-NIR spectra of TIDS derivatives films illustrated that HexylTIDS has the most red-shifted spectrum than those of *i*PrTIDS and EHTIDS (Supporting Information Figure S2). The red shift would be derived from strong $\pi-\pi$ interaction of HexylTIDS molecules in a film state.

The packing structure of HexylTIDS was studied by single-crystal X-ray analysis. Single crystals of HexylTIDS were prepared by the physical vapor transport method using an argon gas flow. The crystals were deep blue fibers. The X-ray analysis revealed columnar structures of π-stacked HexylTIDS, whose interfacial distance was 3.32 Å (Figure 1a). This $\pi-\pi$ distance was slightly shorter than that of *i*PrTIDS (3.40 Å). As shown in Figure 1b, S···O interactions (S1−O1: 2.91 Å and S2−O1: 2.90 Å) and O···H interaction (O2−H2: 2.60 Å) were observed between the columns. Interaction between hexyl chains was also observed in the packing structure. These interactions are likely necessary for forming a herringbone structure of HexylTIDS, which was different from the parallel stacking structure of *i*PrTIDS.[13] Thus, side chain critically affects the manner of packing, and does so in a way that is difficult to predict from the side chain structure. A single crystal of EHTIDS was not obtained because of its poor crystallinity. We consider that the packing structure of TIDS influences its aggregation behavior and photoelectronic properties. Sufficient intercolumnar interactions are necessary for the formation of nanowires in composite films. A shorter $\pi-\pi$ distance will give superior photoelectronic properties.

2. SEM Observation of TIDS:P3HT Composite Films. Next, we prepared composite films containing TIDS and P3HT to investigate nanowires formation of TIDS. Three composite films using *i*PrTIDS, HexylTIDS, and EHTIDS were fabricated with weight ratio of 1:1, and were investigated by SEM to compare the aggregation structures in the films. The SEM images show that *i*PrTIDS:P3HT and EHTIDS:P3HT films had fibers on the surface (Figures 2a and b). We attribute the fibers to steps between aggregated TIDS and P3HT. Both of the films have low density of fibers, indicating that only part of TIDS was aggregated into the fibers structures but most of TIDS was mixed with P3HT into a homogeneous structure. On the other hand, the HexylTIDS:P3HT film exhibited dense fibers like tangled wires (Figure 2c). In a magnified SEM image (Figure 2d), the nanowires were clearly observed to be 50 nm in diameters. This result suggests that the intercolumnar interactions of HexylTIDS shown in Figure 1 are strong enough to form nanowires even in a composite film.

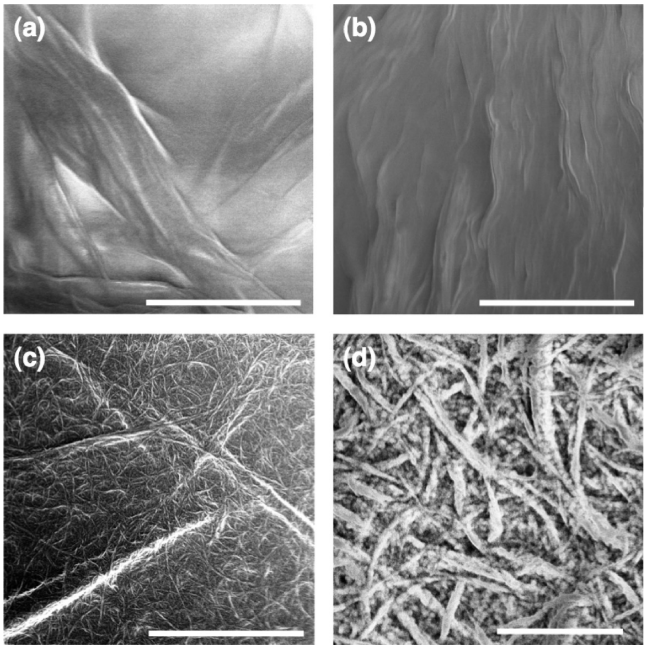

Figure 2. SEM images of TIDS:P3HT films (a) *i*PrTIDS:P3HT (1:1 w/w), (b) EHTIDS:P3HT (1:1 w/w), (c) HexylTIDS:P3HT (1:1 w/w), (d) magnified image for the HexylTIDS:P3HT film. Scale bars are 5 μm in a–c and 400 nm in d.

HexylTIDS formed nanowires in HexylTIDS:$PC_{61}BM$ composite film (1:1 w/w) as well (Supporting Information Figure S4).

The conditions for constructing nanowire structures in the composite films were further investigated by atomic force microscopy (AFM). The observed topographies of HexylTIDS:P3HT films showed that TIDS-rich films formed nanowire structures (Figure 3a–c), whereas the other films with high ratios of P3HT did not exhibit a fibrous morphology (Figure 3d–f). Even in SEM study, we did not observe nanosized structure in a pure P3HT film. Accordingly, we can conclude that the aggregated nanowires were composed of HexylTIDS not P3HT. Furthermore, when *N*-(hexyl)-tetracenecarboxylic acid 5,6-imide was used with P3HT for a composite film in 1:1 w/w ratio, formation of nanowire was not observed (Supporting Information Figure S4). This result represents disulfide unit of TIDS plays an important role to form nanowires in composite films. Prior to this research, the formation of small-molecule nanowires in composite films was unprecedented. According to XRD measurements, HexylTIDS and P3HT formed crystalline phases (Supporting Information Figure S5); however, P3HT did not aggregate into wire-like structures in our conditions probably because the method to fabricate composite films did not contain an aging step for P3HT to transform into wires, while the literature reporting polymer nanowires includes the aging steps prior to fabricating films.[9b,c]

The inherent ability of TIDS to aggregate was examined by comparing SEM images of each TIDS film fabricated by drop casting. The SEM images of *i*PrTIDS, HexylTIDS, and EHTIDS were similar, containing rod-like structures (Figures 4a–c). In a magnified image for the HexylTIDS film, the rods were found to consist of bundles of nanowires (Figure 4d). When capturing SEM images, the *i*PrTIDS film and the EHTIDS film did not give clear accumulated images because of charge-up of the rods, but the HexylTIDS film did. This difference suggests that, in contrast to the *i*PrTIDS and EHTIDS films, the HexylTIDS film has good conductivity that is sufficient for electron transport.

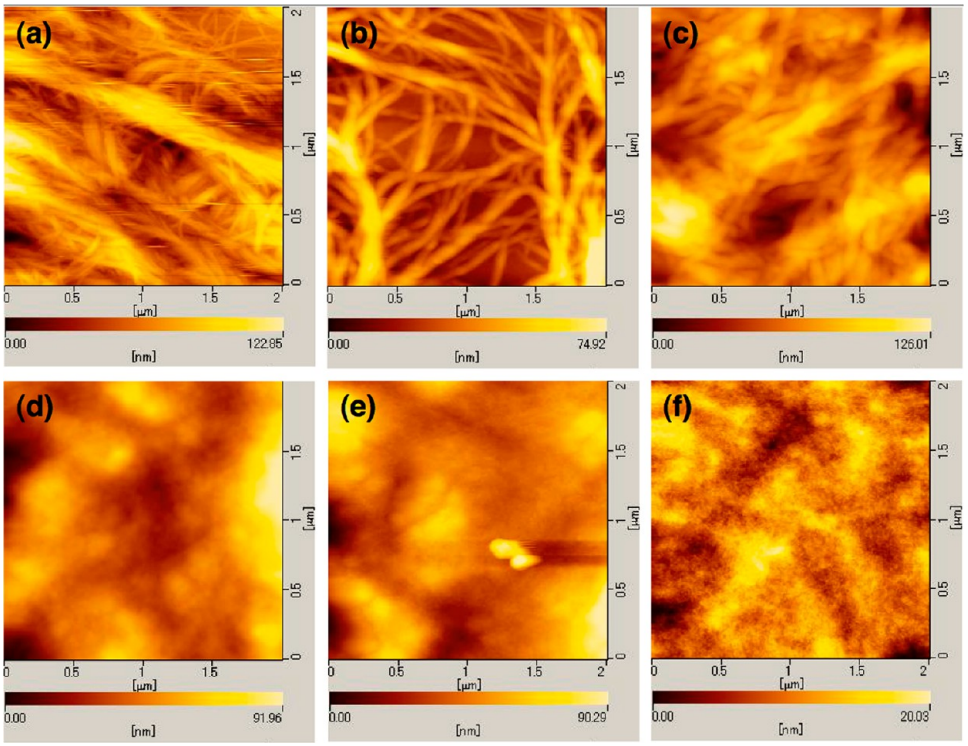

Figure 3. AFM topographies of HexylTIDS:P3HT films. The weight ratios of TIDS and P3HT are (a) 4:1, (b) 2:1, (c) 1:1, (d) 1:2, (e) 1:4, and (f) 0:1.

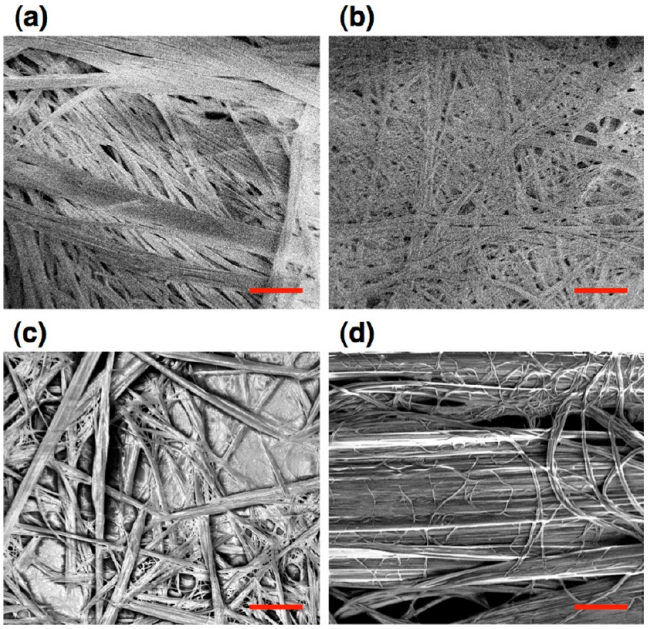

Figure 4. SEM images of TIDS films. (a) *i*PrTIDS and (b) EHTIDS film images are snapshots with 5 μm scale bars. HexylTIDS films images are cumulated pictures with (c) 5 μm scale bar and (d) 400 nm scale bar.

3. Photoconductive Properties of TIDS:P3HT Films. To investigate photoconductive property of nanowires of TIDS in composite film, we conducted flash-photolysis time-resolved microwave conductivity (FP-TRMC) measurements of the TIDS:P3HT thin films.[18] To estimate the films' photoconductivity, the FP-TRMC measurement utilizes laser irradiation onto samples to generate holes and electrons, which absorb microwaves. The FP-TRMC method is advantageous for measuring the photoconductivity of nanowires-like samples,[18b,c] which are difficult to measure by typical methods such as the field effect transistor method and four-probe method.

Comparing the FP-TRMC measurement results, we found that HexylTIDS:P3HT films exhibited much higher photoconductivity than the *i*PrTIDS:P3HT and EHTIDS:P3HT films (Figure 5). In lifetime of carriers, HexylTIDS:P3HT films provided higher values than other TIDS:P3HT composite films (Supporting Information Figure S7). The results clearly denote that nanowires of HexylTIDS in the composite films are crucial for high photoconductivity and long lifetime. The HexylTIDS:P3HT film with the 1:1 w/w ratio gave the highest photoconductivity, which was 2.1×10^{-7} m^2/(V s) (Figure 5), approximately one third of optimized P3HT:[6,6]-phenyl C_{61} butyric acid methyl ester (PCBM) = 1:1 film.[18d] This indicates that HexylTIDS:P3HT in the 1:1 w/w ratio had the best phase separation structure and the most effective conductive paths among all the tested films. It was also evidenced by photoluminescence measurement. HexylTIDS:P3HT film completely quenches photoluminescence of pure P3HT (Supporting Information Figure S3), which suggests that HexylTIDS works as an acceptor in the composite film to increase quantum yield of charge separation resulting in high photoconductivity. This sample with the highest photoconductivity had the weight ratio corresponding to nanowire formation. The decrease in photoconductivity at higher ratios of P3HT corresponds to the AFM images showing no apparent

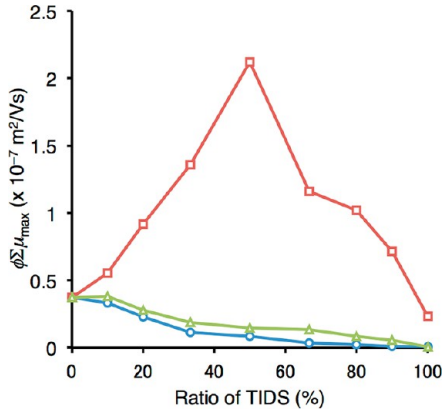

Figure 5. Photoconductivities of TIDS:P3HT films measured by FP-TRMC. Red (square), green (triangle), and blue (circle) lines are corresponding to HexylTIDS:P3HT, EHTIDS:P3HT, and *i*Pr-TIDS:P3HT, respectively. The values are plotted with increasing fractions of TIDS derivatives.

texture (Figures 3d–f). We surmise that excess P3HT disrupts formation of HexylTIDS nanowire, leading to this drop in photoconductivity. On the other hand, low photoconductivity in the films with large amount of HexylTIDS is likely attributed to inefficient phase separation and a small surface area due to the formation of thick and aggregated wires (Figures 3a and b). The films for *i*PrTIDS:P3HT and EHTIDS:P3HT exhibited their highest photoconductivity when 100% P3HT. This data indicates that *i*PrTIDS and EHTIDS do not contribute to free charge carrier generation and transport. This is likely because of their insufficient nanowires formation. Overall, we conclude that formation of TIDS nanowire plays an important role in photoconductivity. Consequently, construction of the nanowire structures, rather than poorly defined structures, in composite films is a promising strategy for realizing higher photoconductivity.

CONCLUSION

We found that a mixture of HexylTIDS and P3HT gave nanowires of HexylTIDS in the composite films. Nanowires formation clearly depended on the choice of TIDS substituent and the weight ratio of components. Notably, intercolumnar interactions (i.e., S···O interaction, O···H interaction, and hexyl–hexyl interaction) played an important role to form nanowires of 50 nm in diameter; the nanowires act to improve photoconductive properties. The results presented here should provide useful information for constructing wire networks of organic semiconductors in thin films for research into organic electronics.

ASSOCIATED CONTENT

Supporting Information

Crystal information file for HexylTIDS. This material is available free of charge via the Internet http://pubs.acs.org.

AUTHOR INFORMATION

Corresponding Author

*E-mail: tokamo@sanken.osaka-u.ac.jp (T.O.); matsuo@chem.s.u-tokyo.ac.jp (Y.M.).

Present Address

[⊥]T.O.: Department of Advanced Electron Devices, Institute of Scientific and Industrial Research (ISIR), 8−1 Mihogaoka, Ibaraki, Osaka 567−0047, Japan.

Notes

The authors declare no competing financial interest.

■ ACKNOWLEDGMENTS

This work was supported by the Funding Program for Next Generation World-Leading Researchers (Y.M.).

■ REFERENCES

(1) (a) Zhao, Y. S.; Zhan, P.; Kim, J.; Sun, C.; Huang, J. *ACS Nano* **2010**, *4*, 1630−1636. (b) Zhang, C.; Zheng, J. Y.; Zhao, Y. S.; Yao, J. *Adv. Mater.* **2011**, *23*, 1380−1384. (c) Yoon, S. M.; Lee, J.; Je, J. H.; Choi, H. C.; Yoon, M. *ACS Nano* **2011**, *5*, 2923−2929. (d) Yan, X.; Li, J.; Möhwald, H. *Adv. Mater.* **2011**, *23*, 2796−2801. (e) Zhao, Y. S.; Xu, J.; Peng, A.; Fu, H.; Ma, Y.; Jiang, L.; Yao, J. *Angew. Chem., Int. Ed.* **2008**, *47*, 7301−7305.

(2) (a) Lee, J.-K.; Koh, W.-K.; Chae, W.-S.; Kim, Y.-R. *Chem. Commun.* **2002**, 138−139. (b) An, B.-K.; Gihm, S. H.; Chung, J. W.; Park, C. R.; Kwon, S.-K.; Park, S. Y. *J. Am. Chem. Soc.* **2009**, *131*, 3950−3957. (c) de Rooy, S. L.; El-Zahab, B.; Li, M.; Das, S.; Broering, E.; Chandler, L.; Warner, I. M. *Chem. Commun.* **2011**, *47*, 8916−8918. (d) Javed, I.; Zhou, T.; Muhammad, F.; Guo, J.; Zhang, H.; Wang, Y. *Langmuir* **2012**, *28*, 1439−1446. (e) Zheng, J. Y.; Yan, Y.; Wang, X.; Zhao, Y. S.; Huang, J.; Yao, J. *J. Am. Chem. Soc.* **2012**, *134*, 2880−2883.

(3) (a) Ma, X.; Li, G.; Wang, M.; Cheng, Y.; Bai, R.; Chen, H. *Chem.—Eur. J.* **2006**, *12*, 3254−3260. (b) Jung, Y. S.; Jung, W. C.; Tuller, H. L.; Ross, C. A. *Nano Lett.* **2008**, *8*, 3776−3780. (c) Zhao, Y. S.; Wu, J.; Huang, J. *J. Am. Chem. Soc.* **2009**, *131*, 3158−3159. (d) Zuo, W.; Quan, B.; Wang, K.; Xia, L.; Yao, J.; Wei, Z. *Small* **2011**, *7*, 3287−3291.

(4) (a) Hu, Z.; Muls, B.; Gence, L.; Serban, D. A.; Hofkens, J.; Melinte, S.; Nysten, B.; Demoustier-Champagne, S.; Jonas, A. M. *Nano Lett.* **2007**, *7*, 3639−3644. (b) Briseno, A. L.; Mannsfeld, S. C. B.; Reese, C.; Hancock, J. M.; Xiong, Y.; Jenekhe, S. A.; Bao, Z.; Xia, Y. *Nano Lett.* **2007**, *7*, 2847−2853. (c) Briseno, A. L.; Mannsfeld, S. C. B.; Lu, X.; Xiong, Y.; Jenekhe, S. A.; Bao, Z.; Xia, Y. *Nano Lett.* **2007**, *7*, 668−675. (d) Tang, Q.; Tong, Y.; Zheng, Y.; He, Y.; Zhang, Y.; Dong, H.; Hu, W.; Hassenkam, T.; Bjørnholm, T. *Small* **2011**, *7*, 189−193. (e) Sarker, B. K.; Liu, J.; Zhai, L.; Khondaker, S. I. *ACS Appl. Mater. Interfaces* **2011**, *3*, 1180−1185.

(5) (a) Zhang, X.; Jie, J.; Zhang, W.; Zhang, C.; Luo, L.; He, Z.; Zhang, X.; Zhang, W.; Lee, C.; Lee, S. *Adv. Mater.* **2008**, *20*, 2427−2432. (b) Che, Y.; Huang, H.; Xu, M.; Zhang, C.; Bunes, B. R.; Yang, X.; Zang, L. *J. Am. Chem. Soc.* **2011**, *133*, 1087−1091. (c) Zhang, Y.; Wang, X.; Wu, Y.; Jie, J.; Zhang, X.; Xing, Y.; Wu, H.; Zou, B.; Zhang, X.; Zhang, X. *J. Mater. Chem.* **2012**, *22*, 14357−14362.

(6) (a) Xin, H.; Kim, F. S.; Jenekhe, S. A. *J. Am. Chem. Soc.* **2008**, *130*, 5424−5425. (b) Wu, P.-T.; Xin, H.; Kim, F. S.; Ren, G.; Jenekhe, S. A. *Macromolecules* **2009**, *42*, 8817−8826. (c) Xin, H.; Reid, O. G.; Ren, G.; Kim, F. S.; Ginger, D. S.; Jenekhe, S. A. *ACS Nano* **2010**, *4*, 1861−1872. (d) Ren, G.; Wu, P.-T.; Jenekhe, S. A. *ACS Nano* **2011**, *5*, 376−384.

(7) (a) Prasanthkumar, S.; Gopal, A.; Ajayaghosh, A. *J. Am. Chem. Soc.* **2010**, *132*, 13206−13207. (b) Babu, S. S.; Prasanthkumar, S.; Ajayaghosh, A. *Angew. Chem., Int. Ed.* **2012**, *51*, 1766−1776.

(8) (a) Chang, C.-Y.; Wu, C.-E.; Chen, S.-Y.; Cui, C.; Cheng, Y.-J.; Hsu, C.-S.; Wang, Y.-L.; Li, Y. *Angew. Chem., Int. Ed.* **2011**, *50*, 9386−9390. (b) Park, J. H.; Carter, A. R.; Mier, L. M.; Kao, C.-Y.; Lewis, S. A. M.; Nandyala, R. P.; Min, Y.; Epstein, A. J. *Appl. Phys. Lett.* **2012**, *100*, 073301.

(9) (a) Yang, X.; Loos, J.; Veenstra, S. C.; Verhees, W. J. H.; Wienk, M. M.; Kroon, J. M.; Michels, M. A. J.; Janssen, R. A. J. *Nano Lett.* **2005**, *5*, 579−583. (b) Kim, J.-H.; Park, J. H.; Lee, J. H.; Kim, J. S.; Sim, M.; Shim, C.; Cho, K. *J. Mater. Chem.* **2010**, *20*, 7398−7405. (c) Kim, J. S.; Lee, J. H.; Park, J. H.; Shim, C.; Sim, M.; Cho, K. *Adv. Funct. Mater.* **2011**, *21*, 480−486. (d) Chen, H.-C.; Wu, I.-C.; Hung, J.-H.; Chen, F.-J.; Chen, I-W. P.; Peng, Y.-K.; Lin, C.-S.; Chen, C.-H.; Sheng, Y.-J.; Tsao, H.-K.; Chou, P.-T. *Small* **2011**, *7*, 1098−1107.

(10) (a) Worfolk, B. J.; Rider, D. A.; Elias, A. L.; Thomas, M.; Harris, K. D.; Buriak, J. M. *Adv. Funct. Mater.* **2011**, *21*, 1816−1826. (b) Yokoyama, D.; Sasabe, H.; Furukawa, Y.; Adachi, C.; Kido, J. *Adv. Funct. Mater.* **2011**, *21*, 1375−1382. (c) Hsu, S.-L.; Chen, C.-M.; Cheng, Y.-H.; Wei, K.-H. *J. Polym. Sci., Part A: Polym. Chem.* **2011**, *49*, 603−611.

(11) (a) Yue, W.; Zhao, Y.; Shao, S.; Tian, H.; Xie, Z.; Geng, Y.; Wang, F. *J. Mater. Chem.* **2009**, *19*, 2199−2206. (b) Kline, R. J.; DeLongchamp, D. M.; Fischer, D. A.; Lin, E. K.; Richter, L. J.; Chabinyc, M. L.; Toney, M. F.; Heeney, M.; McCulloch, I. *Macromolecules* **2007**, *40*, 7960−7965. (c) Facchetti, A.; Mushrush, M.; Yoon, M.-H.; Hutchison, G. R.; Ratner, M. A.; Marks, T. J. *J. Am. Chem. Soc.* **2004**, *126*, 13859−13874. (d) Ong, B. S.; Wu, Y.; Liu, P.; Gardner, S. *J. Am. Chem. Soc.* **2004**, *126*, 3378−3379. (e) Suzuki, Y.; Miyazaki, E.; Takimiya, K. *J. Am. Chem. Soc.* **2010**, *132*, 10453−10466.

(12) (a) Kimura, M.; Watson, W. H.; Nakayama. *J. Org. Chem.* **1980**, *45*, 3719−3721. (b) Lois, S.; Florès, J.-C.; Lère-Porte, J.-P.; Serein-Spirau, F.; Moreau, J. J. E.; Miqueu, K.; Sotiropoulos, J.-M.; Baylère, P.; Tillard, M.; Belin, C. *Eur. J. Org. Chem.* **2007**, 4019−4031. (c) Rašović, A.; Steel, P. J.; Kleinpeter, E.; Marković, R. *Tetrahedron* **2007**, *63*, 1937−1945. (d) González, F. V.; Jain, A.; Rodríguez, S.; Sáez, J. A.; Vicent, C.; Peris, G. *J. Org. Chem.* **2010**, *75*, 5888−5894.

(13) Okamoto, T.; Suzuki, T.; Tanaka, H.; Hashizume, D.; Matsuo, Y. *Chem. Asian J.* **2012**, *7*, 105−111.

(14) (a) Tan, L.; Zhang, L.; Jiang, X.; Yang, X.; Wang, L.; Wang, Z.; Li, L.; Hu, W.; Shuai, Z.; Li, L.; Zhu, D. *Adv. Funct. Mater.* **2009**, *19*, 272−276. (b) Jiang, W.; Zhou, Y.; Geng, H.; Jiang, S.; Yan, S.; Hu, W.; Wang, W.; Shuai, Z.; Pei, J. *J. Am. Chem. Soc.* **2011**, *133*, 1−3. (c) Chiu, C.-Y.; Kim, B.; Gorodetsky, A. A.; Sattler, W.; Wei, S.; Sattler, A.; Steigerwald, M.; Nuckolls, C. *Chem. Sci.* **2011**, *2*, 1480−1486. (d) Liu, Y.; Di, C.-a.; Du, C.; Liu, Y.; Lu, K.; Qiu, W.; Yu, G. *Chem.—Eur. J.* **2010**, *16*, 2231−2239. (e) Qiao, Y.; Wei, Z.; Risko, C.; Li, H.; Brédas, J.-L.; Xu, W.; Zhu, D. *J. Mater. Chem.* **2012**, *22*, 1313−1325.

(15) Pangborn, A. B.; Giardello, M. A.; Grubbs, R. H.; Rosen, R. K.; Timmers, F. J. *Organometallics* **1996**, *15*, 1518−1520.

(16) (a) Laudise, R. A.; Kloc, Ch.; Simpkins, P. G.; Siegrist, T. *J. Cryst. Growth* **1998**, *187*, 449−454. (b) Jurchescu, O. D.; Popinciuc, M.; van Wees, B. J.; Palstra, T. T. M. *Adv. Mater.* **2007**, *19*, 688−692.

(17) Precise description about the parameters are explained in Saeki, A.; Seki, S.; Sunagawa, T.; Ushida, K.; Tagawa, S. *Philos. Mag.* **2006**, *86*, 1261−1276.

(18) (a) Saeki, A.; Koizumi, Y.; Aida, T.; Seki, S. *Acc. Chem. Res.* **2012**, *45*, 1193−1202. (b) Ferguson, A. J.; Blackburn, J. L.; Holt, J. M.; Kopidakis, N.; Tenent, R. C.; Barnes, T. M.; Heben, M. J.; Rumbles, G. *J. Phys. Chem. Lett.* **2010**, *1*, 2406−2411. (c) Saeki, A.; Yamamoto, Y.; Koizumi, Y.; Fukushima, T.; Aida, T.; Seki, S. *J. Phys. Chem. Lett.* **2011**, *2*, 2549−2554. (d) Saeki, A.; Tsuji, M.; Seki, S. *Adv. Energy Mater.* **2011**, *1*, 661−669.